41st European Rotorcraft Forum

A DETAILED BIOMECHANICAL PILOT MODEL FOR MULTI-AXIS INVOLUNTARY ROTORCRAFT-PILOT COUPLINGS

Pierangelo Masarati*, Giuseppe Quaranta*, Andrea Zanoni*

*Dipartimento di Scienze e Tecnologie Aerospaziali, Politecnico di Milano
Via La Masa 34, 20156 Milano – Italy
e-mail: pierangelo.masarati@polimi.it

Abstract

This work presents a complete biomechanical model of the pilot's upper part of the body, which includes the torso, the head and both upper limbs. The model is used to investigate the biodynamic feedthrough, namely the involuntary motion of the control inceptors that is caused by the acceleration of the cockpit. The model is coupled with a detailed multibody model of a helicopter.

1. INTRODUCTION

To successfully accomplish a flight mission task it is necessary for the pilot and the vehicle to cooperate in a joint enterprise. In fact, the pilot and the vehicle form a closed loop system, the so-called "pilot-vehicle system". The closed loop structure ensures in general a good disturbance rejection capability to system. However, in some cases the feedback loop may lead to an instability condition, i.e. to an unfavorable interaction that result in a divergent, often oscillatory, uncontrolled motion. These phenomena are called adverse Rotorcraft Pilot Couplings (RPC) and are often caused by a trigger event that activates the transition to a divergent motion. Classical RPC events are those caused by an erroneous perception of the pilot of the dynamic characteristics of the vehicle. This leads to what is better known as Pilot Induced Oscillations (PIO), which is the effect of a voluntary, out-of-phase, pilot control activity. However, piloted vehicles are also subjected interaction with the pilot caused by the feeding of the vehicle vibrations into the control inceptors that occurs through the biodynamics of the pilot. In this case the divergent oscillation is the result of involuntary control input of the pilot in the loop, and the phenomenon is denominated Pilot Assisted Oscillation (PAO). A practical consequence of this interaction is a modification of the closed loop dynamics of the pilot-vehicle system, which may be perceived as a degradation of the handling qualities of the vehicle, and lead in the worst cases to limit cycle oscillations, excessive loads, and loss of control. Rotorcraft are specifically prone to this problem because they may suffer from higher vibratory loads than fixed wing aircraft, and may present dynamics in the frequency band of biomechanics (2 Hz to 8 Hz, [1]). A review of the recent work done on all types of RPC can be found in these three papers, Refs. [2, 3, 4], where it is reported the work done within the EU sponsored project ARISTOTEL.

The pilot action on the aircraft inceptors is exerted via the forces generated by the muscles driven by the neuromuscular system. The pilot perceives the aircraft position and orientation through the visual and vestibular system; additionally, the proprioception gives the relative position between the pilot's body parts and the neighboring objects with whom he/she is interacting, i.e. the inceptors and all other human machine interface element inserted in the cockpit. Summing up the mechanical impedance of the different parts of the pilot's body between the seat and the inceptors the biodynamic feedthrough (BDFT) is obtained, i.e. the movement of the inceptors grabbed by the pilots due to accelerations of the base. A large variability of the BDFT can be expected, both inter-subject, due

to the different age, size, sex, health and training, and also intra-subject [5]. In fact, the biodynamical properties of the pilot may be influenced by several parameters, which include the posture, the muscular activation, the task and the workload. Most, if not all, are hardly measurable objectively.

A typical approach for the modeling of the biomechanics of the pilot is based on experimentally measured transfer functions. Typically, the pilot biomechanics is dominated by a pair of complex conjugated poles that determine an equivalent mass-spring-damper system. Well known voluntary pilot models (e.g. Hess's structural pilot model, [6]) include a pair of complex conjugated biodynamic poles. Lumped parameter models have been developed for fixed wing aircraft (for example [7, 8]).

In recent times, a detailed, physics based nonlinear multibody model of the left arm of a helicopter pilot has been developed and interfaced with a comparably detailed multibody model of a helicopter to investigate collective bounce [9, 10] (Fig. 1). The

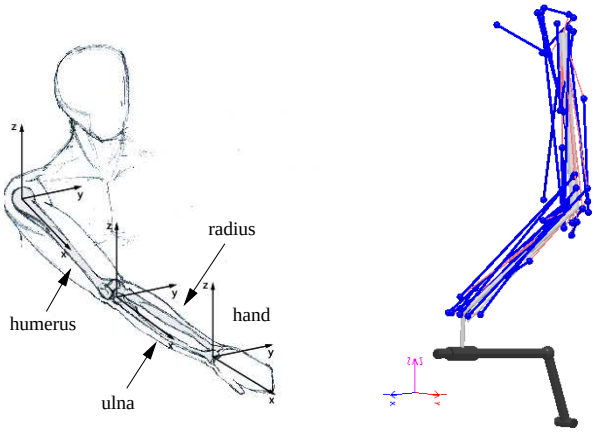

Figure 1: Multibody model of the arm holding the collective control inceptor.

same model was used to identify a linearized, parametric model of the pilot/control device to be used for design purposes [11, 12].

The availability of a detailed, physics based model of the biomechanics of the pilot presents a clear advance with respect to black-box models: as long as it is validated with experimental data, it can be used to analyze and simulate novel cockpit configurations without the need to identify the parameters from dedicated experiments.

2. MODEL DESCRIPTION

This work presents an extension of the previously mentioned biomechanical model of the pilot's left upper limb. The right arm and its interaction with the cyclic control inceptor are modeled, along with the torso. The characteristic properties of closed-loop biodynamic feedthrough and neuromuscular admittance of the right arm are evaluated. The interaction with the torso is discussed.

2.1. Upper human body

The dynamics of the upper body has been recognized as an important element to reconstruct the BDFT of pilots since the initial identification test campaigns performed at the University of Liverpool during the GARTEUR HC AG-16 and the ARISTOTEL projects [2]. In Ref. [13] it is shown how a non-negligible amplification factor of the vertical acceleration transmitted from the seat through the body was measured at pilot's shoulders. Kitazaki and Griffin [14] showed through experiments how it is possible to identify a principal resonance of the human body close to 5 Hz. The associated modal form shows the skeleton that moves vertically due to axial and shear deformation of buttocks tissue, in phase with a vertical visceral mode, and a bending mode of the upper thoracic and cervical spine. Such mode is expected to have a significant effect on the BDFT; consequently, a numerical model of torso was deemed necessary.

The upper body is modeled using a physics based lumped parameters approach, following the idea proposed by Kitazaki and Griffin [15] for a model that only considers motion in the sagittal plane. The model has been transformed back into a three-dimensional one exploiting the database provided by Privitzer and Belytschko [16], whose sagittal plane data was also used by Ref. [15] (Fig. 2(a)). The model is linear; it consists of 34 lumped masses connected by lumped spring elements. The spine is composed by 24 elastic elements made of a linear and a rotational spring positioned between each pair of vertebral bodies representing all intervertebral disks that connect the head to the sacrum. The head is modeled as a single rigid body. In the original model by Kitazaki and Griffin, the intervertebral articulation were modeled as beam elements, allowing a displacement along the sagittal axis between the vertebral bodies which is not compatible with this type of articulation. The masses used to represent the torso are rigidly attached to the upper vertebral bodies with an offset. Instead, the masses of the viscera, below the diaphragm, are represented using 8 concentrated masses. They are separated from those of the spine and connected to them by linear springs along the sagittal direction. This second column of masses was required to keep

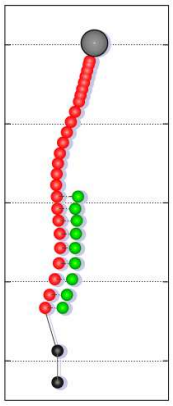

(a) Model of head, spine, pelvis and viscera.

(b) Model of torso coupled with left arm.

Figure 2: Multibody model of torso and left arm holding the collective control inceptor.

into account the larger values associated with the viscera internal organs and the fact that they are not confined by the rib cage. Finally, the pelvis was modeled by a large mass rigidly connected to the sacrum and grounded by two beam elements that model the buttocks tissue.

This detailed model was used to extract low frequency eigensolutions, which are used to produce a reduced order Component Mode Synthesis (CMS) model. The resulting model correlates well with those obtained in Ref. [15] and with the experimental data presented in Ref. [14] (Table 1), at least for the modes that dominate the response when the body is subjected to a vertical oscillation in the vicinity of 5 Hz.

In order to consider the full three-dimensional motion, it was necessary to add the two moments of inertia that were missing from each body, and

Table 1: Characteristic frequencies of the upper body models.

Mode	**[15]** [Hz]	**[14]** [Hz]	**Present** [Hz]
1	0.28	1.10	0.27
2	1.59	2.20	1.78
3	2.81	3.40	3.14
4	5.06	4.90	5.09
5	5.77	5.60	5.99
6	7.51	8.10	7.45

Table 2: Characteristic frequencies of the three dimensional upper body models.

Mode	**Frequency** [Hz]	**Plane**
1	0.29	Sagittal
2	0.94	Coronal
3	1.88	Coronal
4	2.21	Sagittal
5	3.38	Coronal
6	3.89	Coronal
7	4.23	Coronal
8	5.27	Sagittal
9	5.65	Coronal
10	6.27	Sagittal

the torsional and coronal bending elastic connection springs.

The new modal forms obtained were clearly separable into sagittal and coronal, with the sagittal modes that showed a limited modification with respect to those computed with the original two-dimensional model (Table 2).

Finally, the masses associated with the arms that were equally distributed on the nodes of the torso were extracted to prepare the model for connection with the detailed multibody model of the arms' skeletal and muscular system.

2.2. Upper Limbs Biomechanical Model

A multibody model of the upper limbs has been developed, as an extension of the left limb model already presented in earlier works [17, 9, 10], which was derived from the one originally presented by Pennestrì et al. [18]. Each limb consists of four rigid bodies that represent the humerus, the radius, the ulna and the hand. They are connected by ideal kinematic constraints. The total number of degrees of freedom is thus 24. The hand is represented by a single rigid body; a detailed characterization of its muscles was not carried out since the target simu-

lations involve only grasping tasks.

Currently, the shoulder complex is also not modeled in detail, disregarding the clavicle and the scapula. Piloting tasks are typically performed with very low elevation angles of the humerus for both the limbs; therefore the expected effect of the scapula and clavicle motion on the shoulder kinematics is very limited. The glenohumeral joint is represented by a spherical joint located at the glenoid fossa, removing 3 degrees of freedom. A revolute hinge approximates the humeroulnar joint in correspondence to the center of the trochlea, allowing the rotation of the ulna with respect to the humerus only about the local lateral axis. It removes 5 degrees of freedom. The humeroradial joint is represented by a spherical hinge, located at the humeral capitulum, that removes 3 degrees of freedom. The proximal and distal radioulnar joints are modeled by a single inline joint between a point P and the mechanical axis of the ulna. The position of the point is offset from the radius mechanical axis in the lateral direction: the offset is such as to leave the two bones' mechanical axes parallel in the rest position (i.e. with the arm extended anteriorly, the palm facing upward). The original formulation of this kinematic representation of the radioulnar joint is due to Pennestrì et al., more details can be found in [18]. The joint removes 2 degrees of freedom. At its distal end, the radius connects with the hand by means of a cardanic joint, allowing the wrist radioulnar deviation and flexion-extension rotations. It removes 4 more degrees of freedom. As a consequence, the model had 7 degrees of freedom and its kinematics are underdetermined even when the motion of the hand is completely prescribed.

The muscles are modeled using one-dimensional viscoelastic elements whose constitutive laws represent a simplified Hill model, proposed in [18]. The force exerted by a muscle is a function of $x = l/l_0$ and $v = \dot{l}/v_0$, non-dimensional length and normalized velocity of the muscle with respect to reference parameters, and of the voluntary activation a:

$$f = f_0 \left[f_1(x) f_2(v) a + f_3(x) \right] \tag{1}$$

where f_0 is the peak isometric contraction force exerted by the muscle, l_0 represents the length at which f_0 is produced, while v_0 is the maximum contraction velocity of the muscle. Their values are taken from [19]. Tendon compliance is assumed low enough to be disregarded. The total number of muscle bundles modeled is 25 for each limb. Thus, the upper limb multibody model is an underconstrained, overactuated system, since the 25 muscles produce torques acting on the 7 degrees of freedom of the limb.

The muscular activation is a-priori unknown for a given task, depending on the central nervous system control strategy. It can be however estimated by solving a non-linear optimization problem in which the total squared activation $\sum_{i=1}^{n_m} a_i^2$ (n_m being the total number of muscle bundles) is minimized in a given configuration, under the constraint that the torques produced by the muscles must be equal to the ones required to guarantee the dynamic equilibrium of the limb and compliance with the bounds $0 \leq a_i \leq 1$. More details of the complete solution procedure can be found in [9]. The calculated activation values refer to the *passive*, or *involuntary* characteristics of the pilot body. The *active*, or *voluntary* (or better *reflexive*) part of the activation can be estimated by considering a quasi-steady approximation

$$\Delta a = K_p \Delta x + K_d \Delta v \tag{2}$$

such that the force perturbation can be expressed as

$$\begin{aligned} \Delta f = & f_0 \left[\left(f_{1/x} a + f_1 K_p \right) f_2 + f_{3/x} \right] \Delta x \\ & + f_0 f_1 \left(f_{2/v} a + f_2 K_d \right) \Delta v \end{aligned} \tag{3}$$

The baseline for the geometry of the model is represented by the ribcage parametric model presented in [20]: the authors shared a complete dataset comprising the coordinates of 464 landmarks measured on the ribcage of 89 subjects by means of CT scans, along with the results of a PCA (Principal Component Analysis) with respect to the parameters age, sex, stature and Body Mass Index (BMI) of the subject. The most likely ribcage geometry of a subject can be reconstructed on the basis of those parameters. The landmarks representing the other limb segments and joint locations are then inferred by the ribcage dimensions and anthropometric data from [21, 22], to yield the complete geometry of the limbs and their inertial properties.

For the present work, the geometry of the torso model has been considered as reference. Optimal age, sex, stature and BMI of the most likely matching subject have been estimated by minimizing the squared distance of the insertion points of the ribs from their location with respect to the nodes representing the vertebrae in the FEM model of the torso. The resulting pilot is a 34 year old male, of 1.78 m stature and a 26.5 BMI, corresponding to an estimated weight of approximately 84 kg.

The collective control inceptor is modeled as a purely kinematic constraint for the left hand, that holds it in the correct orientation to grasp the

lever and allows its rotation about the global y-axis about the lever hinge location. The choice of not assigning inertial properties to the collective (and cyclic) levers is justified by the wish to isolate the purely biomechanical transfer function of the pilot body with respect to all the external influences and to produce a parametric model of the pilot/control device.

2.3. Right Arm and Cyclic Control Inceptor

The right arm model represents essentially the specular version of the left arm model about the xz-plane with regard to geometry. The inertial properties of the body segments are again set according to the regression analysis published in [21, 22]. The cyclic control inceptor is modeled as an algebraic constraint, this time allowing the rotation of the hand with respect to the cyclic lever hinge location about the global x-axis and about the global y-axis.

2.4. Helicopter Model

The complete biomechanical model of the pilot's upper part of the body is coupled with an aeroelastic model of a medium weight helicopter, with articulated main rotor.

The nonlinear model of the vehicle has been presented in [23], where it was also compared to a linearized state-space (LSS) model of the same vehicle. It is based on the Aerospatiale (now Airbus Helicopters) AS330 Puma. Its analysis within the biomechanical model of the pilot's left arm was originally presented and discussed in [9, 24, 10, 25].

A detailed and complete multibody model of the helicopter has been developed by coupling a detailed aeroelastic model of the main rotor with a structural model of the airframe, a flight mechanics model and dynamic models of the pitch control actuators.

The rotor model features exact kinematics and nonlinear finite element-like structural dynamics thanks to an original finite volume beam formulation [26]. Rotor blade aerodynamics are modeled using the blade element theory, with static aerodynamic coefficients from look-up tables, unsteady aerodynamic correction based on a state-space approximation of Theodorsen's model [27], and global dynamic inflow accounted for using a momentum theory-based model [28]. A detailed view of the main rotor hub is shown in Fig. 3.

The airframe dynamics are modeled using the CMS approach, with eight structural modes, chosen among those in the frequency band up to about 30 Hz that show considerable modal participation of the main and tail rotor, and pilot and co-pilot seats attachment points.

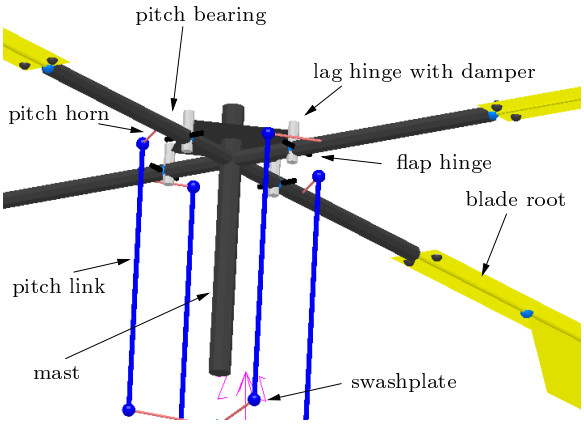

Figure 3: Detailed view of the main rotor hub.

The servoactuators that command the pitch of the main rotor blades are modeled using second-order transfer functions, to provide the appropriate control bandwidth and phase delay between the control device motion and the actual blade pitch.

2.5. Coupled Pilot-Vehicle Model

The coupled multibody pilot-vehicle model is used to assess the integrability of the detailed biomechanical model within a nonlinear aeroservoelastic simulation of the helicopter.

The CMS model of the pilot's torso is connected to the CMS model of the airframe at a location corresponding to the pilot's seat. The inceptors are also connected to the airframe's CMS model relative to the pilot's seat position. The rotation of the inceptors is fed into the main rotor control system in form of signals proportional to the requested swashplate motions, and added to the values required to trim the aircraft and those generated by the SCAS.

3. RESULTS

In the following, results obtained with the proposed detailed multibody model of the pilot are presented. The cockpit geometry is loosely inspired to that of the HELIFLIGHT-R flight simulator in use at the University of Liverpool.

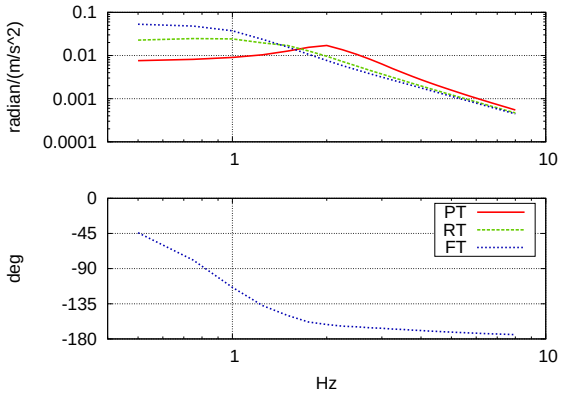

(a) 50% ref. coll., fore/aft excitation

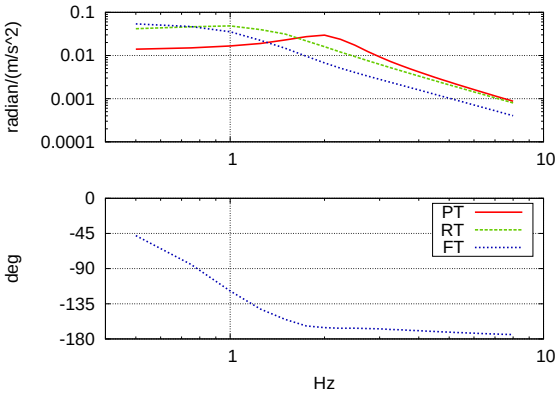

(b) 90% ref. coll., fore/aft excitation

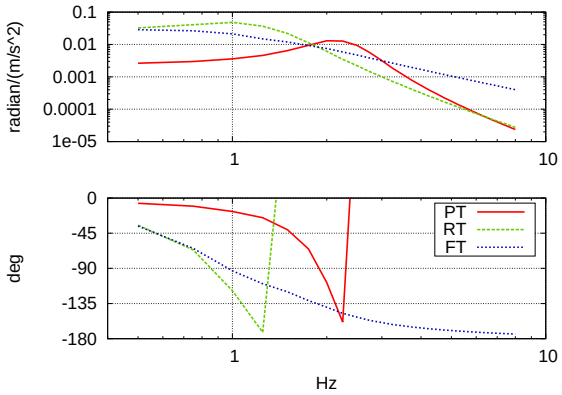

(c) 50% ref. coll., lateral excitation

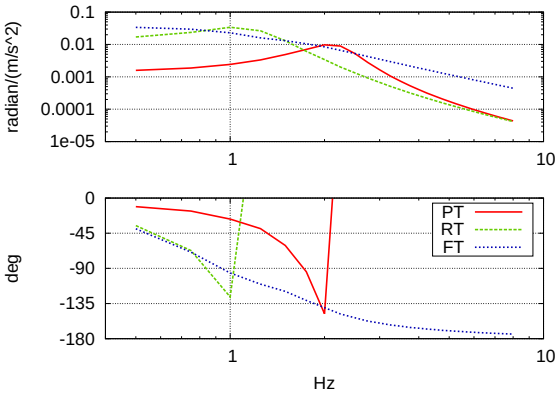

(d) 90% ref. coll., lateral excitation

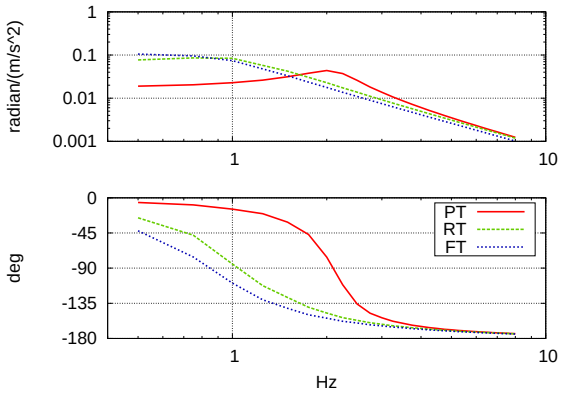

(e) 50% ref. coll., vertical excitation

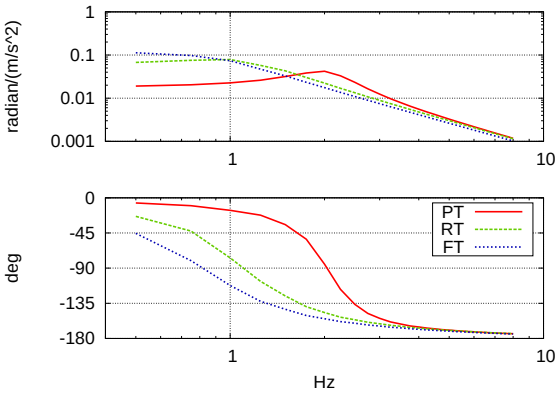

(f) 90% collective, vertical excitation

Figure 4: Collective control inceptor motion for longitudinal, lateral and vertical excitation at 50% and 90% reference collective control for arms only, with PT, FT, RT muscular activation patterns.

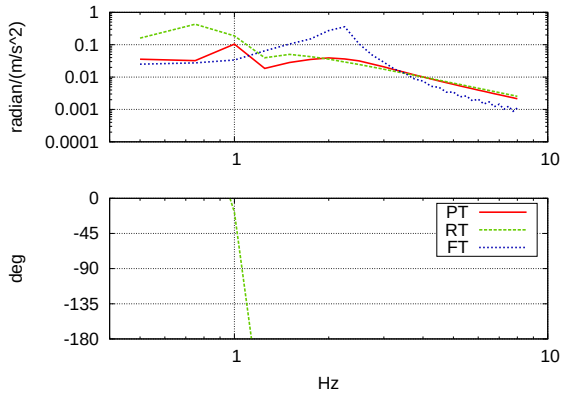

(a) Fore/aft cycl., fore/aft excitation

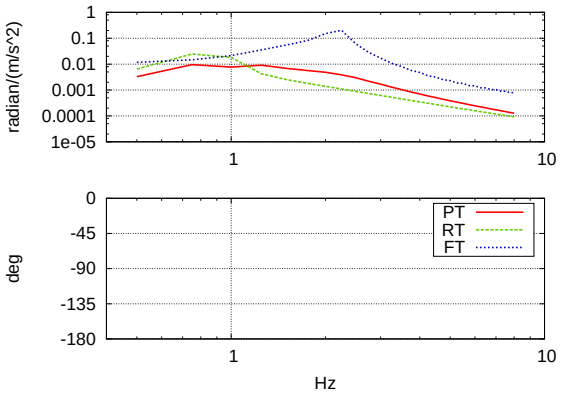

(b) Lateral cycl., fore/aft excitation

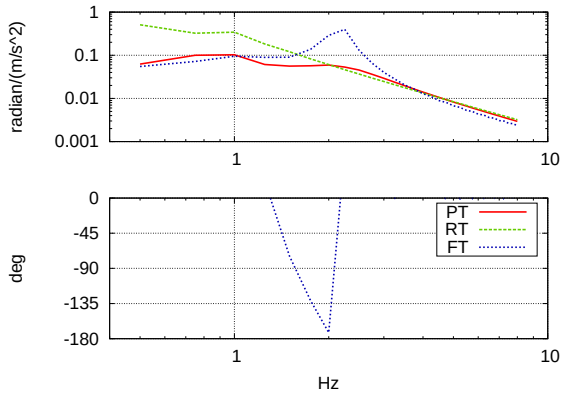

(c) Fore/aft cycl., lateral excitation

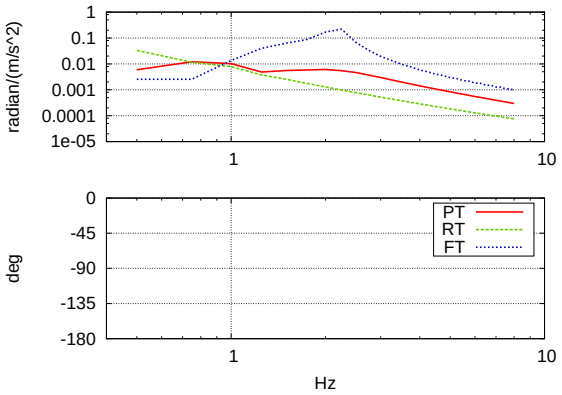

(d) Lateral cycl., lateral excitation

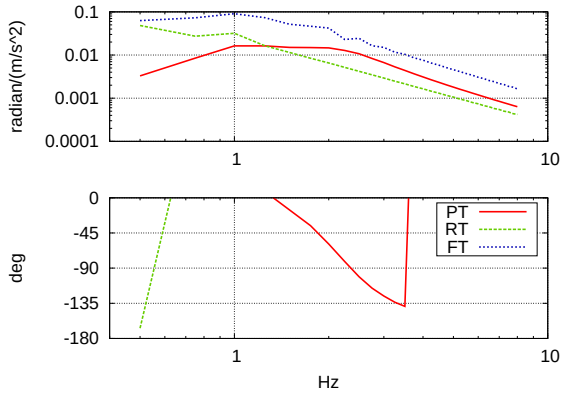

(e) Fore/aft cycl., vertical excitation

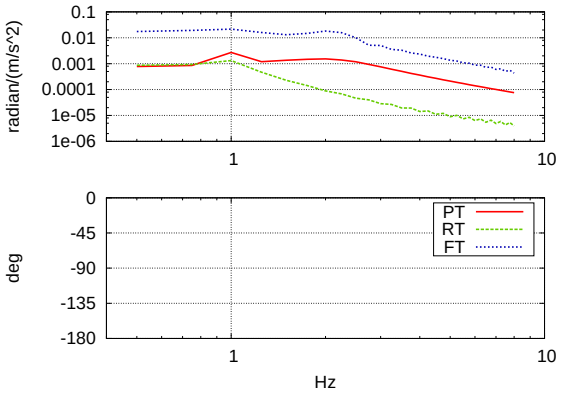

(f) Lateral cycl., vertical excitation

Figure 5: Fore/aft cyclic control inceptor motion for longitudinal, lateral and vertical excitation for arms only, with PT, FT, RT muscular activation patterns.

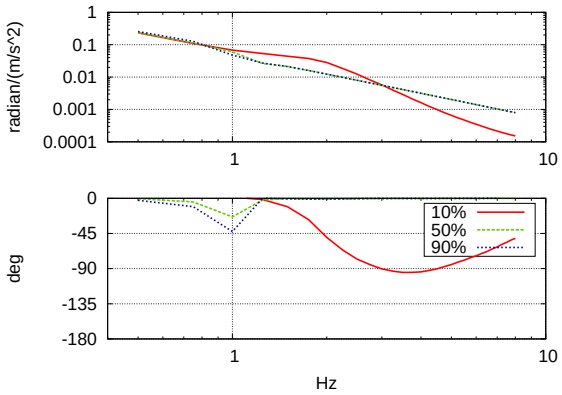

(a) Fore/aft cycl., fore/aft excitation

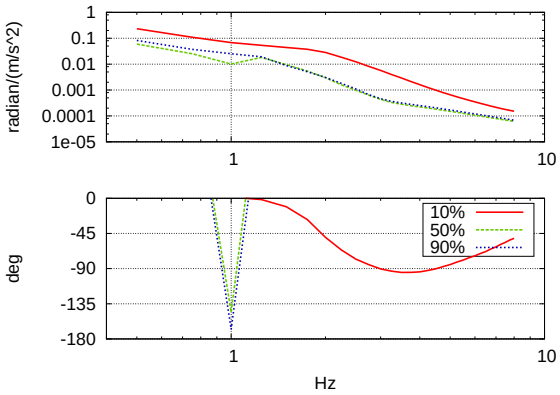

(b) Lateral cycl., fore/aft excitation

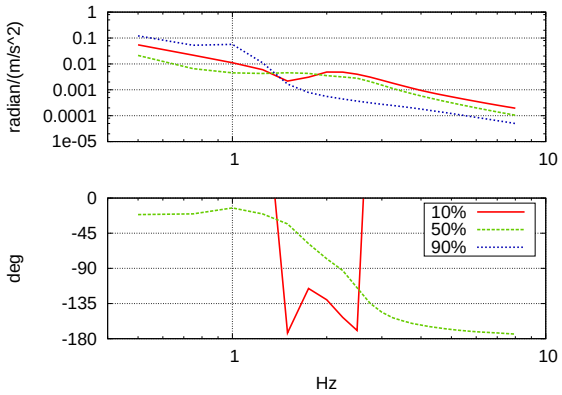

(c) Fore/aft cycl., lateral excitation

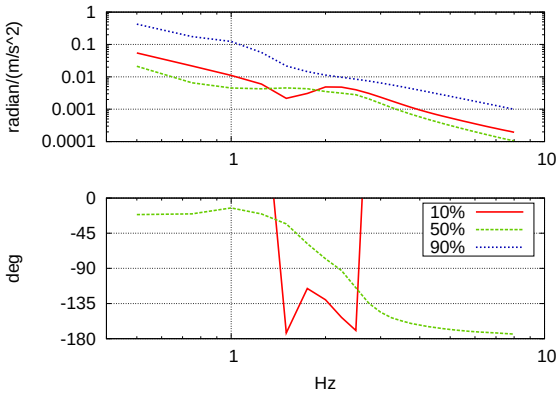

(d) Lateral cycl., lateral excitation

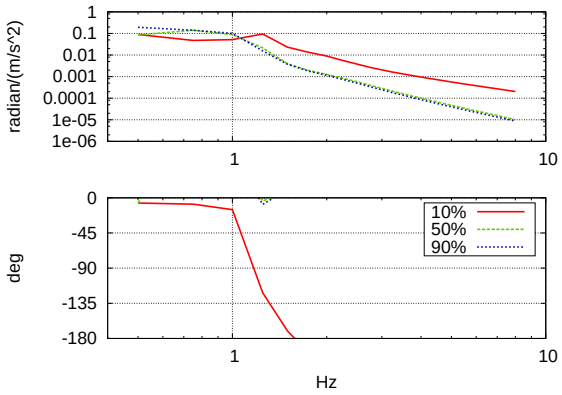

(e) Fore/aft cycl., vertical excitation

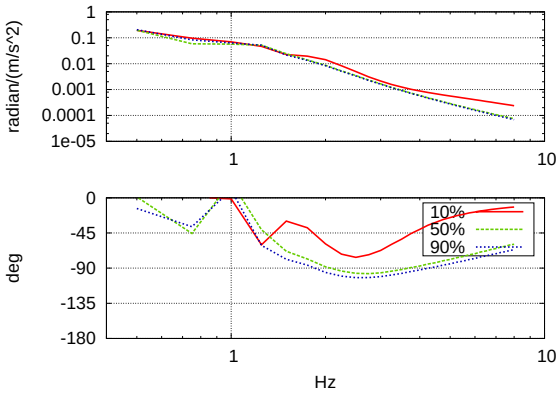

(f) Lateral cycl., vertical excitation

Figure 6: Fore/aft cyclic control inceptor motion for longitudinal, lateral and vertical excitation for arms and torso, with PT muscular activation pattern.

3.1. Involuntary Pilot Action on Collective Control

This section presents the results of the involuntary (and reflexive) action of the pilot on the collective control inceptor that is caused by vibration of the cockpit along the surge, sway, and heave directions. Figure 4 shows the frequency response of the left arm in terms of collective control rotation. Figures (a), (c), and (e), on the left, refer to 50% collective reference position, whereas Figures (b), (d), and (f), on the right, refer to 90% collective reference position. Figures (a) and (b) refer to excitation along the surge direction; Figures (c) and (d) refer to excitation along the sway direction; Figures (e) and (f) refer to excitation along the heave direction. The latter case was already presented and discussed in previous works. Figures (a) to (d) show that collective is also affected by motion in the plane of the vehicle, although the amplitude of the motion is nearly one order of magnitude smaller than that caused by excitation along the heave direction.

3.2. Involuntary Pilot Action on Cyclic Control

This section presents the results of the involuntary (and reflexive) action of the pilot on the cyclic control inceptor that is caused by vibration of the cockpit along the surge, sway, and heave directions. Figure 5 shows the frequency response of the right arm in terms of cyclic control fore/aft and lateral rotation. Figures (a), (c), and (e), on the left, refer to fore/aft rotation, whereas Figures (b), (d), and (f), on the right, refer to lateral rotation. Figures (a) and (b) refer to excitation along the surge direction; Figures (c) and (d) refer to excitation along the sway direction; Figures (e) and (f) refer to excitation along the heave direction. The figures show that the magnitude of both components of cyclic control rotation are similarly influenced by both components of horizontal excitation; excitation along the heave direction provides lower excitation. Analogous results in Figure 6 also include the model of the torso.

3.3. Coupled Pilot-Vehicle Model

Figure 7 shows the motion of the main rotor during Collective Bounce, an instability characterized by the interaction between the main rotor coning motion, the heave motion of the vehicle, and the biodynamic feedthrough of the pilot's left arm holding the collective control inceptor. Collective bounce is encountered after increasing the gearing ratio between the motion of the control inceptor and the swashplate motion to less than twice the nominal value.

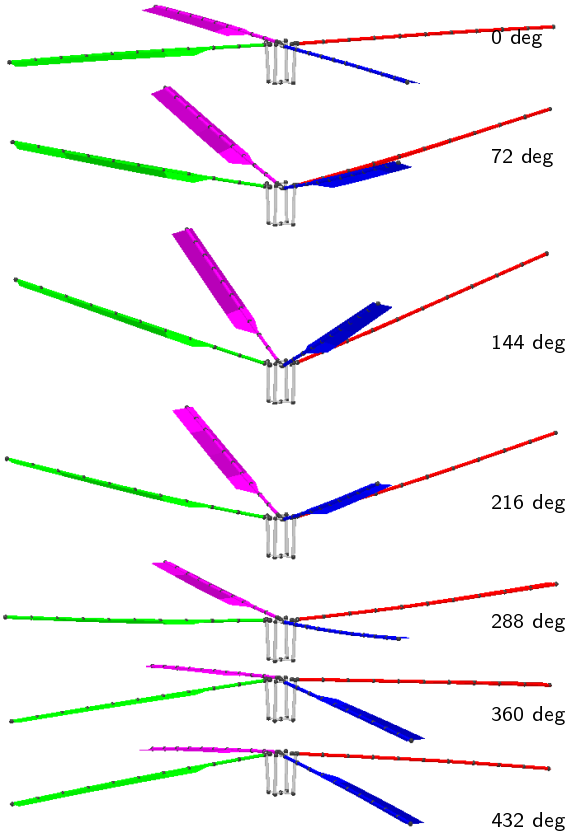

Figure 7: Frames of main rotor motion taken at azimuth increments of 72 deg during a cycle of collective bounce oscillation after the instability developed into a limit cycle oscillation.

Figure 8 presents preliminary results of the same coupled helicopter-pilot model related to motion about the roll axis. The system is perturbed by forcing a lateral cyclic doublet. The 'baseline' response is obtained by not feeding the inceptor rotation into the control system; the 'G=*' responses are obtained by feeding the the inceptor rotation. 'G=1' considers the nominal gearing ratio, whereas 'G=1.6' refers to a gearing ratio 60% larger than nominal. For this problem, no instability is expected.

4. CONCLUSIONS

A biomechanical model of a helicopter pilot's upper portion of the body is presented. The model includes the torso, the head, and both upper limbs. The pilot model is used to characterize biodynamic feedthrough, namely the involuntary motion of the

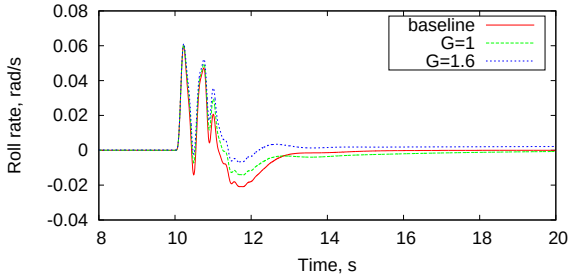

(a) Roll rate

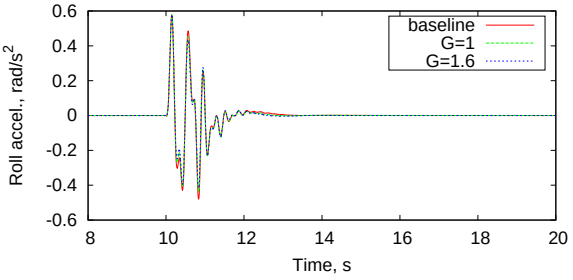

(b) Roll acceleration

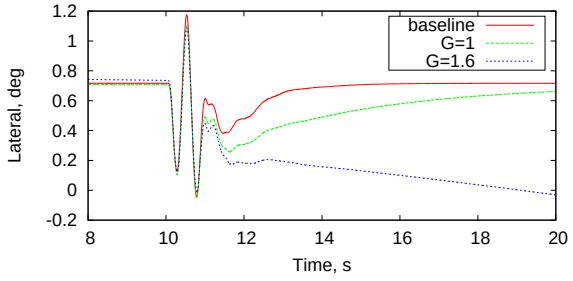

(c) Lateral cyclic rotation

Figure 8: Response to perturbation about the roll axis.

control inceptors that is caused by the acceleration of the cockpit. The pilot model is also coupled with a detailed multibody model of a medium weight helicopter. Coupled simulations are conducted to assess the feasibility of using a detailed pilot model within accurate time marching simulations of detailed helicopter models.

ACKNOWLEDGMENTS

The authors acknowledge the contribution of Mr. Filippo Tunesi to the implementation of the model of the torso. The research leading to these results has received funding from the European Community's Seventh Framework Programme (FP7/2007-2013) under grant agreement N. 266073.

References

[1] O. Dieterich, J. Götz, B. DangVu, H. Haverdings, P. Masarati, M. D. Pavel, M. Jump, and M. Gennaretti. Adverse rotorcraft-pilot coupling: Recent research activities in Europe. In *34th European Rotorcraft Forum*, Liverpool, UK, September 16–19 2008.

[2] Marilena D. Pavel, Michael Jump, Binh Dang-Vu, Pierangelo Masarati, Massimo Gennaretti, Achim Ionita, Larisa Zaichik, Hafid Smaili, Giuseppe Quaranta, Deniz Yilmaz, Michael Jones, Jacopo Serafini, and Jacek Malecki. Adverse rotorcraft pilot couplings — past, present and future challenges. *Progress in Aerospace Sciences*, 62:1–51, October 2013. doi:10.1016/j.paerosci.2013.04.003.

[3] Marilena D. Pavel, Pierangelo Masarati, Massimo Gennaretti, Michael Jump, Larisa Zaichik, Binh Dang-Vu, Linghai Lu, Deniz Yilmaz, Giuseppe Quaranta, Achim Ionita, and Jacopo Serafini. Practices to identify and preclude adverse aircraft-and-rotorcraft-pilot couplings — a design perspective. *Progress in Aerospace Sciences*, 76:55–89, 2015. doi:10.1016/j.paerosci.2015.05.002.

[4] Marilena D. Pavel, Deniz Yilmaz, O. Stroosma, Binh Dang-Vu, Pierangelo Masarati, Giuseppe Quaranta, Massimo Gennaretti, Michael Jump, Linghai Lu, Michael Jones, Hafid Smaili, and Larisa Zaichik. Practices for identifying and precluding adverse aircraft- and rotorcraft-pilot couplings events — simulator guidelines. *Progress in Aerospace Sciences*, in press. doi:10.1016/j.paerosci.2015.05.007.

[5] M. J. Griffin. *Handbook of Human Vibration*. Academic Press, London, 1990.

[6] R. A. Hess. Theory for aircraft handling qualities based upon a structural pilot model. *J. of Guidance, Control, and Dynamics*, 12(6):792–797, 1989. doi:10.2514/3.20483.

[7] Henry R. Jex and Raymond E. Magdaleno. Biomechanical models for vibration feedthrough to hands and head for a semisupine pilot. *Aviation, Space, and Environmental Medicine*, 49(1–2):304–316, 1978.

[8] Gordon Höhne. Computer aided development of biomechanical pilot models. *Aerospace Science and Technology*, 4(1):57–69, January 2000. doi:10.1016/S1270-9638(00)00117-6.

[9] Pierangelo Masarati, Giuseppe Quaranta, and Andrea Zanoni. Dependence of helicopter pilots' biodynamic feedthrough on upper limbs' muscular activation patterns. *Proc. IMechE Part K: J. Multibody Dynamics*, 227(4):344–362, December 2013. doi:10.1177/1464419313490680.

[10] Pierangelo Masarati and Giuseppe Quaranta. Bioaeroservoelastic analysis of involuntary rotorcraft-pilot interaction. *J. of Computational and Nonlinear Dynamics*, 9(3):031009, July 2014. doi:10.1115/1.4025354.

[11] Stefano Zanlucchi, Pierangelo Masarati, and Giuseppe Quaranta. A pilot-control device model for helicopter sensitivity to collective bounce. In *ASME IDETC/CIE 2014*, Buffalo, NY, August 17–20 2014. DETC2014-34479.

[12] Pierangelo Masarati, Giampiero Bindolino, and Giuseppe Quaranta. A parametric pilot/control device model for rotorcraft biodynamic feedthrough analysis. In *40th European Rotorcraft Forum*, Southampton, UK, September 2–5 2014.

[13] Pierangelo Masarati, Giuseppe Quaranta, and Michael Jump. Experimental and numerical helicopter pilot characterization for aeroelastic rotorcraft-pilot couplings analysis. *Proc. IMechE, Part G: J. Aerospace Engineering*, 227(1):124–140, January 2013. doi:10.1177/0954410011427662.

[14] Satoshi Kitazaki and Michael J. Griffin. Resonance behaviour of the seated human body and effects of posture. *Journal of Biomechanics*, 31(2):143–149, February 1998. doi:10.1016/S0021-9290(97)00126-7.

[15] Satoshi Kitazaki and Michael J. Griffin. A modal analysis of whole-body vertical vibration, using a finite element model of the human body. *Journal of Sound and Vibration*, 200(1):83–103, February 1997. doi:10.1006/jsvi.1996.0674.

[16] Eberhardt Privitzer and Ted Belytschko. Impedance of a three-dimensional head-spine model. *Mathematical Modelling*, 1(2):189–209, 1980. doi:10.1016/0270-0255(80)90037-8.

[17] Andrea Zanoni, Pierangelo Masarati, and Giuseppe Quaranta. Upper limb mechanical impedance variability estimation by inverse dynamics and torque-less activation modes. In P. Eberhard and P. Ziegler, editors, *2nd Joint International Conference on Multibody System Dynamics*, Stuttgart, Germany, May 29–June 1 2012.

[18] E. Pennestrì, R. Stefanelli, P. P. Valentini, and L. Vita. Virtual musculo-skeletal model for the biomechanical analysis of the upper limb. *Journal of Biomechanics*, 40(6):1350–1361, 2007. doi:10.1016/j.jbiomech.2006.05.013.

[19] K. R. S. Holzbaur, W. M. Murray, and S. L. Delp. A model of the upper extremity for simulating muscoloskeletal surgery and analyzing neuromuscular control. *Annals of Biomechanical Engineering*, 33:829–840, 2005.

[20] X. Shi, L. Cao, M Reed, J. Rupp, C. Hoff, C. Hoff, and J. Hu. A statistical human rib cage geometry model account for variations by age, sex, stature and body mass index. *Journal of Biomechanics*, 47:2277–2285, 2014.

[21] James Cheverud, Claire C. Gordon, Robert A. Walker, Cashell Jacquish, Luci Kohn, Allen Moore, and Nyuta Yamashita. 1988 anthropometric survey of US Army personnel: correlation coefficients and regression equations. part 1: Statistical techniques, landmark, and mesurement definitions. TR 90/032, NATICK, 1990.

[22] James Cheverud, Claire C. Gordon, Robert A. Walker, Cashell Jacquish, Luci Kohn, Allen Moore, and Nyuta Yamashita. 1988 anthropometric survey of US Army personnel: correlation coefficients and regression equations. part 4: Bivariate regression tables. TR 90/035, NATICK, 1990.

[23] Vincenzo Muscarello, Pierangelo Masarati, and Giuseppe Quaranta. Multibody analysis of rotorcraft-pilot coupling. In P. Eberhard and P. Ziegler, editors, *2nd Joint International Conference on Multibody System Dynamics*, Stuttgart, Germany, May 29–June 1 2012.

[24] Pierangelo Masarati and Giuseppe Quaranta. Coupled bioaeroservoelastic rotorcraft-pilot simulation. In *Proceedings of ASME IDETC/CIE*, Portland, OR, August 4–7 2013. DETC2013-12035.

[25] Pierangelo Masarati, Giuseppe Quaranta, Andrea Bernardini, and Giorgio Guglieri. A multibody model for piloted helicopter flight dynamics and aeroservoelasticity. *J. of Guidance, Control, and Dynamics*, 38(3):431–441, 2015. doi:10.2514/1.G000837.

[26] Gian Luca Ghiringhelli, Pierangelo Masarati, and Paolo Mantegazza. A multi-body implementation of finite volume beams. *AIAA Journal*, 38(1):131–138, January 2000. doi:10.2514/2.933.

[27] J. Gordon Leishman. *Principles of Helicopter Aerodynamics*. Cambridge University Press, Cambridge, UK, 2nd edition, 2006.

[28] Dale M. Pitt and David A. Peters. Theoretical prediction of dynamic-inflow derivatives. *Vertica*, 5(1):21–34, 1981.